CHALMERS
UNIVERSITY OF TECHNOLOGY

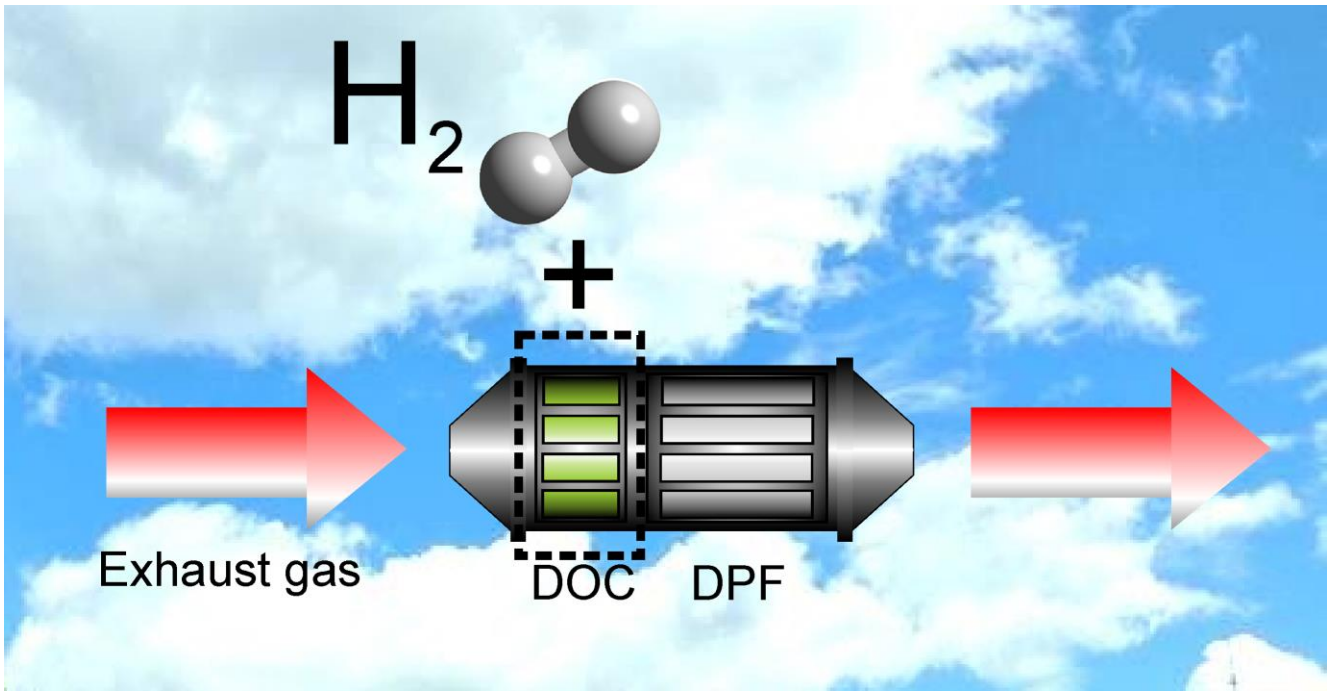

Microkinetic Modeling of Promotional Effects of H2 for Diesel Oxidation Catalyst

Master's thesis in Chemical Engineering

SÉBASTIEN PISSOT

Department of Chemistry and Chemical Engineering
CHALMERS UNIVERSITY OF TECHNOLOGY
Gothenburg, Sweden 2014

Table of Contents

Abstract

With an aim to increase the performance of the diesel oxidation catalyst to achieve gas emissions in compliance with regulations, Herreros *et al.* (2014) have reported a promotional effect of H_2 on NO oxidation over Pt/Al_2O_3. This effect has been further investigated by Azis *et al.* (2015), and H_2 was proposed to retard platinum oxide formation at low temperature, leading later to enhanced NO_2 yield at higher temperature. In this thesis work, a micro-kinetic model using data from literature is developed in order to test how well it simulates Azis *et al.* (2015) experiments, with a focus on NO/O_2 mixtures and $NO/O_2/CO$ mixtures. For NO/O_2 mixtures, the model, including up to 34 elementary-like reaction steps, 9 gas species and 9 adsorbed species is implemented in a simple single channel reactor model of the catalytic monolith. Mass and heat balances are kept simple, without mass transfer, and no parameter fitting. The model is found to predict the higher light-off temperature with increasing H_2 concentration found experimentally, though the promotional effect of H_2 at high temperature (above 300˚C) is not predicted correctly. Delay in platinum oxide formation due to H2 is also predicted by the model, and can be explained by surface coverages effects, with adsorbed nitrogen denying oxygen adsorption at low temperature. However, the platinum oxide formation is most likely over estimated by the model, as are nitrogen and N_2O production. Furthermore, the model is used to simulate $NO/O_2/CO$ mixtures by adding 14 reactions and 4 adsorbed species. The model then predicts much higher light-off temperature for both CO and NO oxidation than experimentally observed. Besides, it failed to predict a promotional effect of H_2 on CO oxidation, predicting actually the opposite. These findings show that the model needs to be improved, for instance by including mass transport and monolith radial discretization. Parameter fitting should be done to simulate more precisely Azis *et al.* (2015) experiments, and reactions step could be added or modified.

1. Introduction

With growing concern to contain global warming, reduce fuel consumption and improve urban air quality, a lot of attention has recently been focused on emissions aftertreatment for rich gasoline and lean diesel engine. The major pollutants targeted by regulations such as the Clean Air Act in the US and the European emission standard (currently Euro 6) in Europe, are CO, hydrocarbons, Nitrogen oxides (NOx) and particles. For an ordinary gasoline engine, with a near stoichiometric ratio between air and fuel, the three way catalyst can effectively reduce emissions for these pollutants (Granger and Parvulescu, 2011). However, with lean-burn gasoline and diesel engine, which are bound to become the dominant combustion engine types, the conventional three-way catalyst is not as effective due to the excess of O_2. Therefore, a lot of improvement is needed in the design of lean-burn engine emission abatement systems.

The catalytic abatement system for lean-burn and diesel engines is generally made of three parts: the Diesel Oxidation Catalyst (DOC), the Diesel Particle Filter (DPF) and the NOx reduction catalyst which generally carries out a Selective Catalytic Reduction (SCR) where NOx is converted to N2. The purpose of the DOC is to oxidize CO, hydrocarbons and organic fractions of particulate matter. Furthermore, it facilitates the oxidation of NO to NO2, which later on enhances particle oxidation in the DPF unit and is favorable for the SCR when NH3 is used as reductant. Hence it is very interesting to enhance NO oxidation in the DOC. Herreros *et al.* (2014) have reported that addition of H2 improves NO oxidation over the DOC, and that this effect is not only due to the exothermic effect of H2 oxidation. M.M.Azis (2015) has further investigated this effect with various gas mixtures and has investigated the time-scale the effect of H2 addition with these mixtures in transient experiments. Herreros *et al.* (2014) used an actual diesel engine exhaust for their study, while Azis (2015) used a synthetic exhaust gas, allowing for greater variation in the exhaust composition. From his study, H2 was found to enhance CO and hydrocarbon oxidation at low temperature and hinder platinum oxide formation at low temperature, leading subsequently to higher NO_2 yield at higher temperature. The purpose of this thesis work was to build a kinetic model and analyze how well it simulates the experimental results, based on the experiments and results from M.M.Azis et al. (2015). The model was built in a step-by–step fashion, first with only NO oxidation reactions and then H_2 and CO oxidation reactions over platinum were added. A steady-state model was first used, and then once the kinetic model was found robust enough, a transient model was developed.

When it comes to kinetic modeling of NO oxidation in Selective catalytic reduction or in NOx storage reduction, often elementary-like kinetic models are used (Mahzoul et al. 1999 ; Olsson et al. 2001 ; Li et al. 2003). These so called micro-kinetic models are useful to describe and simulate precisely the behavior of a system over a relatively broad range of conditions and explain the chemistry behind experimental observations. However they require a large number of parameters and can be computationally demanding and less robust. Conversely, a few global kinetic models have been published (Mulla et al. 2005 ; Olsson et al. 2005 ; Hauptmann et al. 2007) which require much less computational power but their validity is limited to a much smaller range of conditions.

The model in this thesis work was built with the goal of simulating NO oxidation over Pt/Al_2O_3 over a broad range of experimental conditions, and had to be able to predict results beyond the experimental conditions tested by Azis *et al*.. The other main purpose of this model was to understand how the

surface chemistry might contribute to the observed promotional effect of H_2 on NO oxidation. Therefore, a micro-kinetic model was chosen to be built. Most publications do not share the value of the kinetic parameters used in their models, and when they do they are often limited to a relatively small number of elementary-like steps (Olsson et al. 2001). Eventually, our model was based on a very extensive and widely cited model in the literature developed by Koop and Deutschmann (2009).

This thesis work will focus on implementing Koop and Deutschmann (2009) model to Azis (2015) experiments, for NO/O_2 and $NO/O_2/CO$ gas mixtures, and investigate how well the model fits the experiments and describes H_2 promotional effect. The kinetic parameters Koop and Deutschmann (2009) propose will not be modified, and no parameter fitting will be carried out for this work.

2. Experimental methods

No experiments were conducted for this thesis work, however, the model was developed around the experiments conducted by M.M.Azis et al. (2015). The detailed method of preparation of the catalyst will not be discussed here, only a brief summary of the catalyst properties will be described.

2.1 Catalyst preparation

The catalyst powder contains 1 wt.% Pt which was prepared by wet impregnation on alumina (Al_2O_3). The catalyst was then deposited as a washcoat on a honeycomb structured monolith, which was 2 cm long, with a diameter of 2 cm. The cell density of the monolith was 400 cpsi (channel per square inch). The catalyst powder was calcinated for two hours to remove impurities. The platinum dispersion was measured to be approximately 2% by CO chemisorption, as described by Auvray (2013).

2.2 Flow reactor experiments

The experiments were conducted in a tubular quartz flow reactor heated by an electric coil. Two thermocouples measure the temperature. One was placed inside the monolith at approximately 0.5 cm from the outlet, which indicated the outlet or catalyst temperature. The other one is placed 1 cm before the inlet of the monolith and indicated the gas inlet temperature.

2.3 Experiments

Azis et al. (2015) conducted two main types of experiments: Temperature-programmed reaction (TPR) experiments and transient experiments. The purpose of Temperature-programmed reaction experiments was to study the effect of hydrogen for various gas mixtures with varying temperature. This was achieved by ramping up the temperature of the reactor to 500°C with a rate of 5°C/min, then holding for 5 min the temperature at 500°C, and then finally ramping down the temperature to 120°C with the same rate.

Azis et al. (2015) also investigated the temporal build-up of platinum oxide and how it was affected by hydrogen. Transient experiments were conducted for CO/O2 mixtures with or without 750 ppm H_2, by heating first from 120˚C to 230˚C during approximately 1000 seconds (with a rate of 5˚C/min) and then holding at 230˚C for 1h.

Each experiment was preceded by a catalyst pretreatment under oxidative dry atmosphere, with 10% O_2 in Ar at 450˚C for 20mins. This was followed by a reductive dry atmosphere with 2% H_2 at the same temperature for 30mins.

In this thesis work, focus was put mostly on experiments with a gas mixture of NO/O_2 with varying concentration of H_2, with Argon used as gas balance. H_2O was also present in the gas mixture. The exact inlet composition used by Azis *et al.* (2015) for the NO/O2 mixture is described in Table 1:

Table 1: NO/O2 gas mixtures composition

Gas	NO	O2	H2O	H2
Concentration	500 ppm	8%	5%	0-250-500-750-1000 ppm

Though the focus in this thesis was put on NO/O2 gas mixtures, NO/O2/CO mixtures were also simulated. The composition of the mixture is described in Table 2.

Table 2: NO/O2/CO gas mixtures composition

Gas	NO	CO	O2	H2O	H2
Concentration	500 ppm	200 ppm	8%	5%	0-250-500-750-1000 ppm

3. Model building

3.1 Reactor Model

The reactor used by M.M.Azis (2015) for his experiments was a monolith-supported catalyst, which was simulated as only one single channel, divided into several tanks in series. The model was kept simple, without any mass or heat transport equations; hence the washcoat was not discretized in the radial direction.

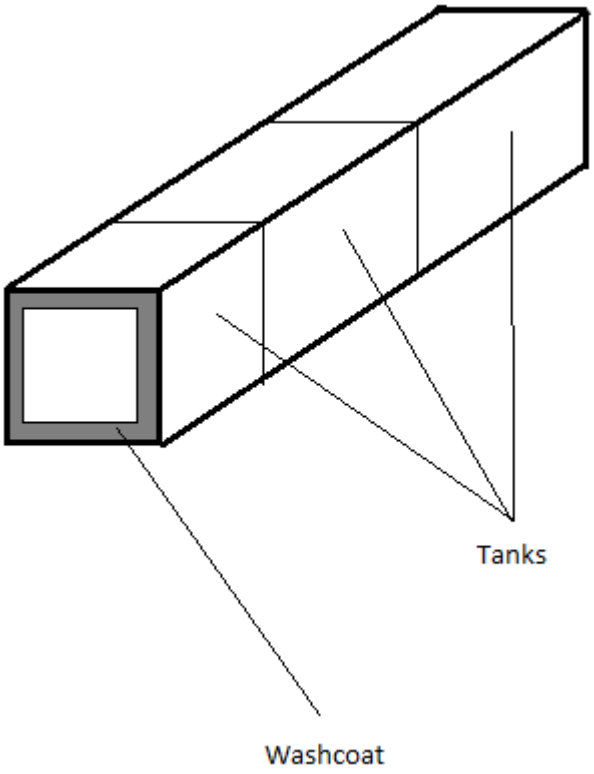

Figure 1: Tank in series channel model

Theoretically, the number of tanks required can be estimated with dispersion model for laminar flow in an open-open system (Folger 2006; Azis 2015), however such an estimation was not performed for this thesis work, instead a number of 10 tanks was used, allowing for a relatively fine discretization without dramatic increase of computational time.

3.2 Micro-kinetic approach

When building a kinetic model, two approaches can be used: macro-kinetic or micro-kinetic approaches. The macro-kinetic -or global- approach combines adsorption, desorption and surface reaction into one global reaction rate expression. This kind of model can be built on the assumption that one step is the rate determining step and all other steps are in equilibrium. Conversely, micro-kinetic model are based on multiple elementary steps without any assumption regarding a possible rate determining step (Thybaut et al., 2002). As the purpose of this thesis work is to build a computer model in order to gain better understanding of the mechanisms of the H_2 effect on DOC, a micro-kinetic model is preferred.

The micro-kinetic model used for the simulation of DOC is based on a very detailed model from Koop and Deutschmann (2009). The original model consists of 73 elementary-like reaction steps between 22 adsorbed species and 11 gas phase species.

The reactions rates are written as follow:

$$r_j = k_j * \prod_{i=1}^{Ngas} {y_i}^{\nu_i} * \prod_{k=1}^{Nads} {\theta_k}^{\nu_k} \qquad \text{Equation 1}$$

With G the number of gas phase species involved in reaction j, y_i the molar fraction of component I in gas phase, ν_i the stoichiometric coefficient of specie i in reaction j, S the number of adsorbed species involved in reaction j, θ_k the surface coverage of specie k and ν_k the stoichiometric coefficient of adsorbed specie k in reaction j. The reaction constant k_j is determined from a simple Arrhenius Law:

$$k_j = A_j * e^{\frac{-Ea_j}{R*T}} \qquad \text{Equation 2}$$

With A_j the pre-exponential factor for reaction j, Ea_j the activation energy for reaction j, T the temperature and R the gas constant. Values for pre-exponential factors and activation energy were obtained from literature.

Koop and Deutschmann model (2009) used surface reaction rates in $mol.m^{-2}.s^{-1}$ calculated from gas phase concentration rather than mole fraction and surface concentrations rather than surface coverages. Therefore, values for pre-exponential factors were given in $cm^2.mol^{-1}.s^{-1}$ for surface reactions following a Langmuir-Hinshelwood mechanism and in s^{-1} for desorption. In order to obtain reaction rates in s^{-1} for all reaction, reaction constant k were to be converted to s^{-1} as well. Bimolecular surface reaction rates were converted multiplying by the surface site density in $mol_{Pt}.cm^{-2}{}_{exposed\ Pt}$, which is an intrinsic parameter for the catalyst. In the case of platinum over alumina, its value is $2.72*10^{-9}$ (Koop and Deustchmann, 2009). For NO oxidation, most authors assume an Eley-Rideal mechanism where NO in gas phase reacts with adsorbed oxygen, however, indications for a Langmuir-Hinshelwood reaction step can be found in literature (Olsson et al., 2001), Koop and Deustchmann (2009) chose to build a model combining both mechanisms. The pre-exponential factor for this reaction was given in $cm^3.mol^{-1}.s^{-1}$ and was converted to s^{-1} by multiplication with the total gas phase concentration. The activation energy was given in kJ/mol.

Kinetic parameters for adsorption were determined by setting the activation energy to 0 and calculating the pre-exponential factor thanks to the sticking coefficient for given specie at 0 coverage. The formula used is taken from Kumar et al. (2006) and gives the rate constant in s^{-1}:

$$k_i = S_{o,i} * \frac{C_{Pt}}{\Gamma} * \sqrt{\frac{RT}{2\Pi M_i}} \qquad \text{Equation 3}$$

$S_{o,i}$ is the sticking coefficient for specie k at 0 coverage, Γ is the surface site density aforementioned, C_{Pt} is the mole of exposed Platinum per unit volume of catalyst, which value was taken assuming the catalyst used here has roughly the same properties as Kumar *et al*. (2011). The value for C_{Pt} is 27,7 $mol_{exposed\ Pt}/m^3_{catalyst}$ and is taken as is from Kumar et al. (2011). T is a reference temperature which value was taken equal to 600 K (Olsson *et al.* (2001)) and M_i is the molar mass of specie i.

3.2.1 NO/O2 gas mixtures

In total, the model uses 34 reactions steps: 7 adsorption reactions, 7 desorption reactions, 18 surface reactions and 2 platinum oxide reactions. All kinetic data were taken from Koop and Deutschmann (2009), aside from platinum oxide formation and decomposition reactions, which were taken from Hauptmann *et al* (2009). The platinum oxidation reaction used is based on formation from NO_2 rather than to O_2 as the oxidative power of NO_2 is much higher. Dissociation of platinum oxide is due to the reductive effect of NO. The oxidized form of platinum modelled by Hauptmann *et al.* (2009) is Pt-O, however, Olsson and Fridell (2002) as well as Després *et al.* (2006) report formation of both Pt-O and Pt-O_2. Furthermore, it is assumed that oxidized platinum site are completely inactive, however it might be

that their activity is actually instead inexistent. Indeed, Wang et al. (2009) have shown that NO activity is lower on Pt-O_2 compared to Pt, but not inexistent.

Table 3: Reactions and their kinetic parameters for NO/O_2 mixtures

Reaction	Number	Pre-exponentail factor s^{-1}	Activation energy kJ/mol
Adsorption Reactions			
$NO + * \Rightarrow NO*$	1	1.408e8	0
$NO_2 + * \Rightarrow NO_2*$	2	1.204e8	0
$O_2 + 2* \Rightarrow 2O*$	3	1.123e7	0
$H_2O+* \Rightarrow H_2O*$	4	1.604e8	0
$H_2+2* \Rightarrow 2H*$[1]	5	2.952e7	0
$N_2O + * \Rightarrow N_2O*$	6	3.420e6	0
$N_2 + 2* \Rightarrow 2N*$	7	1.715e5	0
Desorption Reactions			
$NO* \Rightarrow NO + *$	8	2.1e12	80.7
$NO_2* \Rightarrow NO_2 + *$	9	1.40e13	61
$2O* \Rightarrow O_2 + *$	10	8.7e12	224.7 - 120θ(O)
$H_2O* \Rightarrow H_2O+*$	11	5.00e13	49.2
$H* + H* \Rightarrow 2* + H_2$	12	5.71e12	69.1 - 6θ(H)
$N_2O* \Rightarrow N_2O + *$	13	1.2e10	0.7
$N* + N* \Rightarrow 2* + N_2$	14	1.01e13	113.9
Surface Reactions			
NO oxidation reactions			
$NO* + O* \Rightarrow NO_2* + *$	15	3.54e8	133 + 75θ(CO)
$NO + O* \Rightarrow NO_2*$	16	~3.6e8	113.3 - 60θ(O) + 75θ(CO)
$NO_2* + * \Rightarrow NO* + O*$	17	2.20e10	58
$NO_2* \Rightarrow NO + O*$	18	3.30e14	115.5
$NO_2* + H* \Rightarrow NO* + OH*$	19	1.06e13	20
$NO* + OH* \Rightarrow NO_2* + H*$	20	1.66e14	175.3
$N* + NO* \Rightarrow N_2O + *$	21	1.36e12	90.9
$N_2O* + * \Rightarrow NO* + N*$	22	7.89e15	133.1
$NO* + * \Rightarrow N* + O*$	23	1.36e12	107.8 + 33θ(CO)
$N* + O* \Rightarrow NO* + *$	24	2.72e12	122.6
$N* + OH* \Rightarrow NO* + H*$	25	1.74e13	99.9
$H* + NO* \Rightarrow N* + OH*$	26	3.26e12	25 + 80θ(CO)
Hydroxide formation			
$H* + O* \Rightarrow OH* + *$	27	1.01e12	70.5
$OH*+* \Rightarrow H*+O*$	28	2.72e12	130.7
$OH*+H* \Rightarrow H_2O*+*$	29	1.01e13	17.4
$H2O*+* \Rightarrow OH*+H*$	30	1.85e12	67.6
$OH* + OH* \Rightarrow H_2O* + O*$	31	1.01e13	48.2

[1] The reaction order with respect to vacant sites was set to 1 by Koop and Deutschmann (2009), as opposed to the stoichiometry.

H_2O*+O*==>OH*+OH*	32	6.80e11	38.2
Platinum oxide formation			
NO_2* => Pt-Ox + NO	33	3.80e3	32
Pt-Ox + NO => NO_2*	34	~0.7479	0

3.2.2 $NO/O_2/CO$ gas mixtures

As mentioned in the experimental section, $NO/O_2/CO$ mixtures were also investigated, 14 reactions were added to the previous model, with 4 additional adsorbed species. The reactions and their kinetic parameters are described in Table 4:

Table 4: Reactions and their kinetic parameters for $NO/O_2/CO$ mixtures

Reaction	Number	Pre-exponentail factor s^{-1}	Activation energy kJ/mol
Adsorption Reactions			
CO + * => CO*	35	1.392e8	0
CO2 + * => CO2*	36	3.248e5	0
	Desorption Reactions		
CO* => CO + *	37	2.1e13	136.2 - 33θ(CO)
CO2* => CO2 + *	38	3.6e10	23.7
Surface Reactions			
CO oxidation reactions			
CO* + O* => CO2* + *	39	1.01e12	108 + 90θ(NO) - 33θ(CO)
CO2* + * => CO* + O*	40	1.09e13	165.6 + 60θ(CO)
C* + O* => CO* + *	41	1.01e13	0 + 33θ(CO)
CO* + * => C* + O*	42	4.6e12	205.4 + 60θ(O)
CO* + OH* => HCOO* + *	43	1.01e13	94.2
HCOO* + * => CO* + OH*	44	3.54e12	0.9
HCOO* + O* => OH* + CO2*	45	1.01e13	0
OH* + CO2* => HCOO* + O*	46	7.62e12	151.1
HCOO* + * => H* + CO2*	47	1.01e13	0
H* + CO2* => HCOO* + *	48	7.62e12	90.1

3.3 Mass balance equations

As mentioned previously, mass transport between gas and solid phase was not included in this model, instead a simple mass balance for each tank coupling gas phase and catalyst surface was used. The mass balance for specie i in tank k is:

$$\left(F_{i,k} - F_{i,k-1}\right) = \left(\sum_{j=1}^{N_R} r_{j,k} * \nu_{i,j}\right) * \frac{C_{site} * m_{cat,k}}{N_A} \qquad \text{Equation 4}$$

With $F_{i,k-1}$ the inlet flow of species i in tank k, $F_{i,k}$ the outlet molar flow of species i out of tank k, $r_{j,k}$ the rate of reaction j (in s^{-1}) in tank k, $\nu_{i,j}$ the stoichiometric coefficient of species i in reaction j, C_{site} the site

density of catalyst in sites/mg, calculated for 1 wt.% Pt with 2% dispersion, $m_{cat,k}$ the mass of catalyst in tank k and N_A the Avogadro number.

The adsorbed species transient balance is:

$$\frac{d\theta_{i,k}}{dt} = \sum_{j=1}^{N_R} r_{j,k} * \nu_{i,j} \qquad \text{Equation 5}$$

And the site conservation equation:

$$\theta_{v,k} = 1 - \sum_{i=1}^{Nads} \theta_{i,k} \qquad \text{Equation 6}$$

With $\theta_{i,k}$ surface coverage of adsorbed specie i in tank k, $\theta_{v,k}$ surface coverage of vacant sites in tank k.

3.4 Heat balance equations

A simple heat balance was implemented in the program to account for heat of reactions, heat loss to the environment (simulated as heat radiation). The heat balance for tank k is written as follow:

$$\begin{aligned} & F_{tot,k} C_{p,gas}\left(T_{g,k-1} - T_{g,k}\right) + \left(\sum_{j=1}^{N_R} r_{j,k}(-\Delta H_{r,j})\right) \frac{C_{site} m_{cat,k}}{N_A} \\ & - U_{tot} \frac{m_{cat,k}}{m_{cat,tot}} \left({T^4}_{g,k} - {T^4}_{\infty}\right) \\ & = C_{p,monolith} \left(m_{monolith} \frac{m_{cat,k}}{m_{cat,tot}} + m_{cat,k} \right) \frac{dT_{g,k}}{dt} \end{aligned} \qquad \text{Equation 7}$$

With $F_{tot,k}$ the total molar flowrate in tank k (reacting gas phase and inerts), $\Delta H_{r,j}$ the reaction enthalpy of reaction j, U_{tot} a radiation heat transfer coefficient set equal to $18.5*10^{-12}$ W/K^4 and T∞ the environment temperature set to 150 ˚C.

Instead of including the heat of reaction of every reaction steps, only the heat of reaction for the two most important global reactions was included. Therefore, the enthalpy of reaction for the reaction: NO + O => NO_2* was set to -58.19 kJ/mol (58.19 kJ/mol for reverse reaction) for both Langmuir-Hinshelwood and Eley-Rideal mechanisms (reaction 15 and 16 respectively). The heat of reaction for H_2O formation (reactions 29 and 31) reactions was set to -243.8 kJ/mol (243.8 kJ/mol for reverse reactions 30 and 32). These heats of reaction correspond to a reference temperature equal to 250˚C. These heats of reaction correspond to the global reaction heats (from gas phase reactants to gas phase products) at a reference temperature equal to 250˚C. The enthalpy of reaction of every other reaction step was set to 0. This information is summed up in Table 5.

Table 5: Heat of reactions

Reaction	Reaction enthalpy (KJ/mol)
NO* + O* => NO_2* + *	-58.19
NO_2* + * => NO* + O*	58.19
NO + O* => NO_2*	-58.19
NO_2* => NO + O*	58.19
OH*+H* ==> H_2O*+*	-243.8

H2O*+*==>OH*+H*	243.8
OH* + OH* ==> H_2O* + O*	-243.8
H_2O*+O*==>OH*+OH*	243.8

Heat losses by conduction to the environment as well as axial conduction through the monolith length are not included in this heat balance, which is kept as simple as possible.

3.5 Model limitations

As stated previously, the channel model was kept simple and a lot of factors were neglected. In reality, all reactions do not occur on the washcoat surface, but through the washcoat, meaning that diffusion of species through the washcoat layers should be included if the aim is to develop a more realistic model. Often, the washcoat is discretized in both the axial and radial direction. Mass transport resistance from gas phase to the washcoat and from the washcoat to gas phase has also been neglected. For the heat balance model to be more realistic, the heat of reaction for every reaction should be included, as well as convection from the gas phase, heat conduction through the monolith length and heat losses by convection with the environment.

Concerning the microkinetic model, though it is quite extensive, it might not be extensive enough or not represent reality accurately enough. For instance, Rankovic *et al.* (2011) use more steps for the coupling reactions between CO and H_2 and more coupling between gas phase and platinum surface whereas Koop and Deutschmann (2009) include more reactions that couple H2 and NO oxidation. However, increasing the number of reactions and adsorbed species leads to an increase in computational time.

3.6 MatLab program

Two MatLab® programs were built and used in this thesis. The first one is a steady-state program which simulates for one experimental point only and was mainly used for testing the kinetic model. The second program is a transient simulation program which uses mainly the same body as the first program, but can simulate experiments such as temperature-programmed reaction experiments.

The layout of the transient program is described in Figure 23 in appendix III.

The main file is simulate.m, which calls the functions that set up the simulation (fysdata, expdata, kinetics, simpdef and catdata) then solve the differential equations through function calcest and finally plots the relevant results calling the function plotter. Table 7 (appendix II) describes what every function in the program does and their outputs. The functions are described in the order they are called in the program.

In the case of the steady-state program, the only structural difference in the program is that there is no need to call ODEcalc_init. When heat balance is implemented into the transient program, the layout remains the same, only a differential equation is added in ODEcalc_init and ODEcalc files. The steady-state program solves the system of differential and algebraic equations from given start conditions until Equation 5 is lower than a set threshold value (1e-5 in this case). When this threshold is reached, the rate of change of the surface coverages is considered low enough for steady states to have been reached. The transient program, however, works in two steps. First, in ODEcalc_init, similar to the steady-state program it solves for steady-state conditions at the time zero experiment conditions. Then, it solves the system of differential and algebraic equations for the remaining time steps.

When using a detailed model with reversible reaction steps, some of the reaction steps can be very close to the equilibrium, which can make simulation stiff and computationally demanding. Therefore, the average value of a reversible reaction rate pair is limited to be no more than a set order of magnitude (1e3 in this work) higher than the net difference in that reaction pair. This allowed the program to run faster and avoid stiffness.

3.7 Parameter fitting

The goal of this thesis work was primarily to test existing micro-kinetic models and try to simulate and explain experimental results from the existing models rather than developing our own models. Consequently, no parameter fitting was performed, the only ''parameter tuning'' consisted in adjusting the pre-exponential factor and activation energy of the reverse NO oxidation reaction (reaction 17 & 18) so that the simulation of NO_2 formation was thermodynamically consistent. Also, the platinum dispersion in the model was adjusted in order for NO2 yield to better fit the experiment in the kinetic regime.

4. Results

4.1 Temperature

To be consistent with Azis *et al.* (2015) results, both experimental and simulated results were plotted against the catalyst outlet temperature, measured as explained in the experimental section.

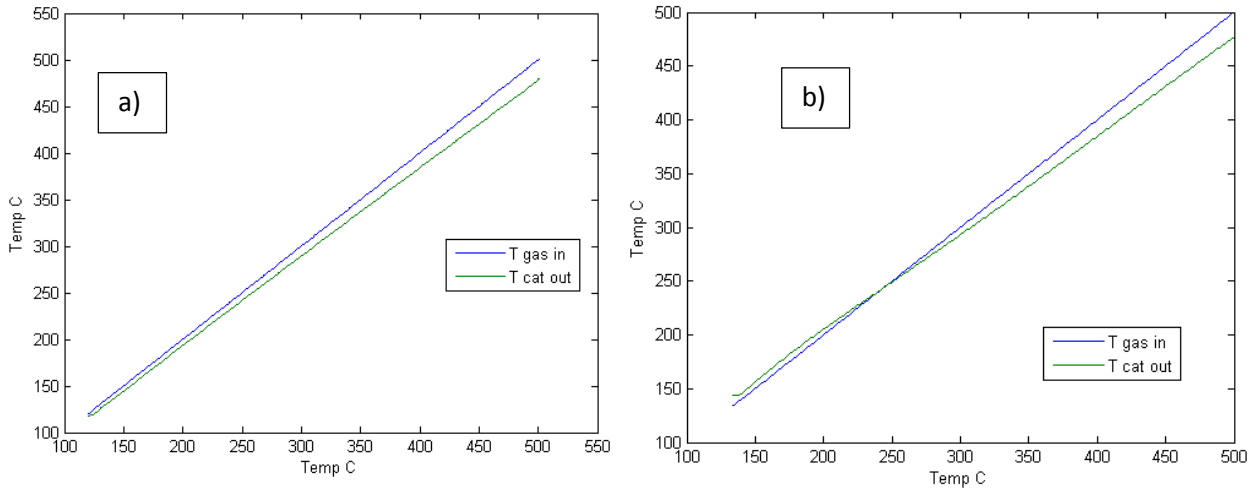

Figure 2: Comparison of inlet gas temperature and catalyst outlet temperature for NO/O_2 gas mixture experiment. (a) No H_2 in feed. (b) 1000ppm H_2 in feed. Plotted versus gas inlet temperature exceptionally.

It can be seen from Figure 2 that with or without H_2, the temperature of the catalyst is not equal to the temperature of the inlet. Besides, when H_2 is fed, the temperature of the monolith is first higher than the temperature of the inlet gas, and then becomes lower at around 230˚C, with H_2 being fully converted around 200˚C. The difference between the catalyst temperature and the gas inlet temperature is mainly due to two factors: first, there are temperature gradients along the length of the catalyst resulting from heat losses, and second is the temporal lagging behind of catalyst temperature, due to thermal inertia. The adiabatic temperature rise for the experiment with NO oxidation only was

estimated to be 1.0˚C for 80% conversion. For NO oxidation with H_2 (1000ppm) oxidation, with 80% conversion for NO and 100% conversion for H_2, the adiabatic temperature rise was estimated to be 12˚C. Consequently, assuming the temporal effect is negligible due to the slow ramping rate 5˚C/min, if the reactor was adiabatic the catalyst temperature should be slightly higher than the gas inlet temperature. This is not the case, proof that there are some heat losses and that the reactor is not adiabatic.

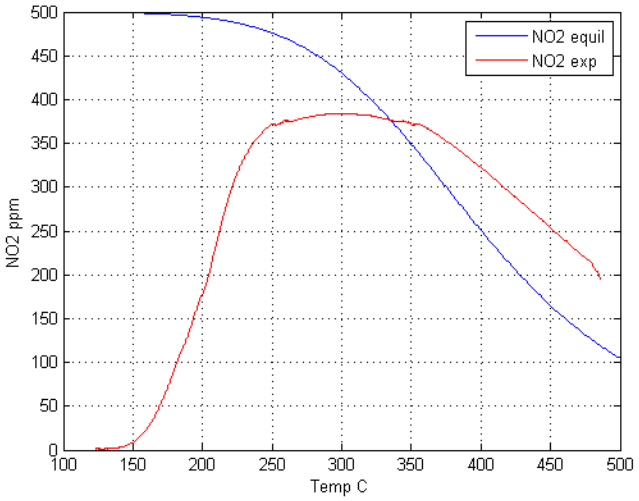

Figure 3: Comparison of NO_2 yield from experiment and equilibrium for NO/O_2 gas mixture experiment with 750ppm H_2 in feed.

Figure 3 shows that between 120 and 300˚C, NO_2 formation is controlled by kinetics, but from approximately 350˚C, thermodynamic equilibrium is causing decrease in NO_2 yield. There is a 20˚C to 60˚C difference between the thermodynamic curve and the experimental curve in the thermodynamic control regime as can be seen in Figure 3. The experimental curve being above the equilibrium curve means that the actual catalyst temperature is lower than the one measured, mainly due to heat losses. Obviously, any kinetic model that is thermodynamically constrained can predict only a maximum NO2 yield, limited by thermodynamic at a given temperature. Therefore, this difference must be accounted for in order for the model to fit the experiment with more accuracy, which is done by adding the differential equation shown in Equation 7. By doing so, the simulated NO_2 yield can be made to follow much closer the experimental equilibrium as can be seen in Figure 4.

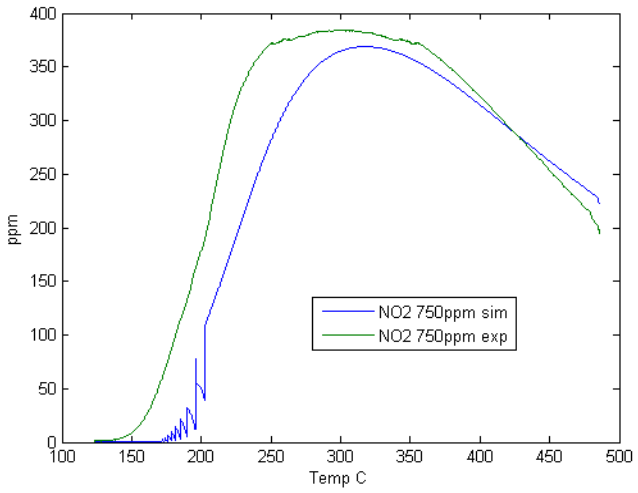

Figure 4: Comparison of NO_2 yield from simulation and experiment for NO/O_2 gas mixture experiment ,with heat balance, 750ppm H_2 in feed.

As can be seen from Figure 4, the simulation is close to the experiment at temperature higher than 350˚C when equilibrium limited. Without the heat balance, the simulated curve in Figure 4 would be closer to the equilibrium curve from Figure 3.

4.2 Platinum oxide dispersion

As mentioned previously, the Platinum dispersion of the catalyst in Azis *et al.* (2015) experiments was reported to be 2%. However, it appeared that when simulating with 5% dispersion, the simulation results are much closer to the experimental results in the kinetic regime (ca. 120-300˚C), as can be seen in Figure 5. Both these results were obtained accounting for heat balance.

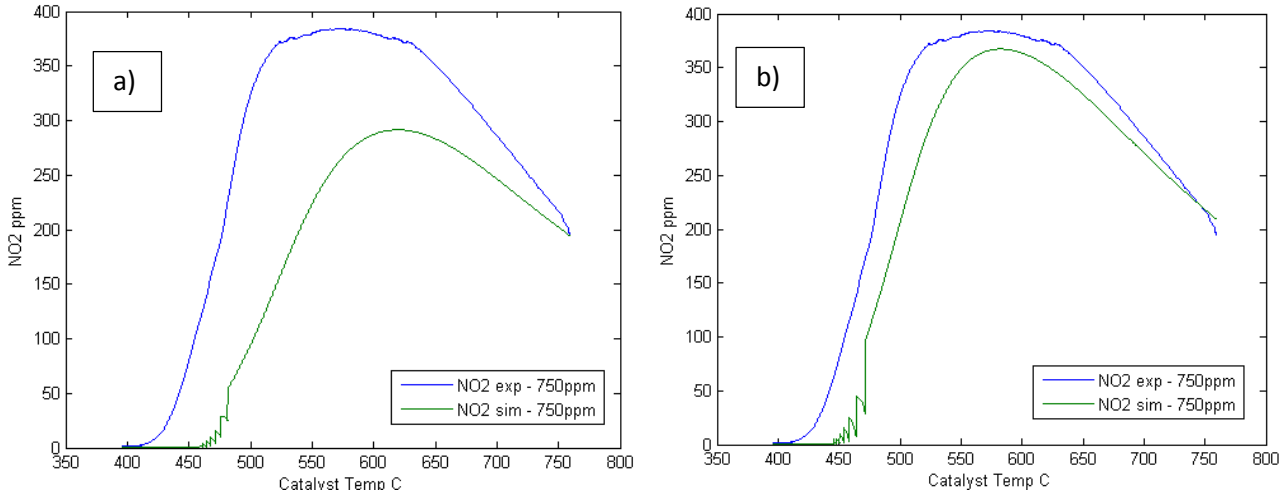

Figure 5: Comparison of experimental and simulated NO2 yield for NO/O_2 gas mixture experiment, for 2% platinum dispersion (a) and 5% platinum dispersion (b)

This 5% dispersion value was fixed totally arbitrarily, no optimization was performed on this value and most likely there is another value which would give better results. However, this thesis work was more focused on the micro-kinetic model rather than on the simulation parameter, hence the 5% value was considered sufficient.

Consequently, the results that are going to be presented subsequently will be simulated with 5% platinum dispersion on accounting for heat balance.

4.3 Effect of H_2 on NO/O_2 gas mixtures

Azis *et al.* found that at low temperature (below 200˚C), H_2 addition had a negative effect on NO_2 yield. Mixtures with H_2 in feed were found to have a higher light-off temperature as can be seen in Figure 6. NO_2 concentration is plotted against the catalyst temperature (measurement near the end of the monolith) as to reduce the impact of H_2 exothermal effect on H_2 promotional effect. Between 200-300˚C, H_2 was found to increase NO_2 yield with increasingly positive effect with higher H_2 concentration, up to 750ppm. However, for 1000ppm H2, NO_2 yield started to decrease. Above 300˚C NO_2 yield decreased, but NO_2 yield remained higher with H_2 in feed, and increasingly with H_2 concentration. In this temperature range, thermodynamic is controlling, hence differences are not due to H_2 influencing kinetics, but H_2 might be changing equilibrium conditions.

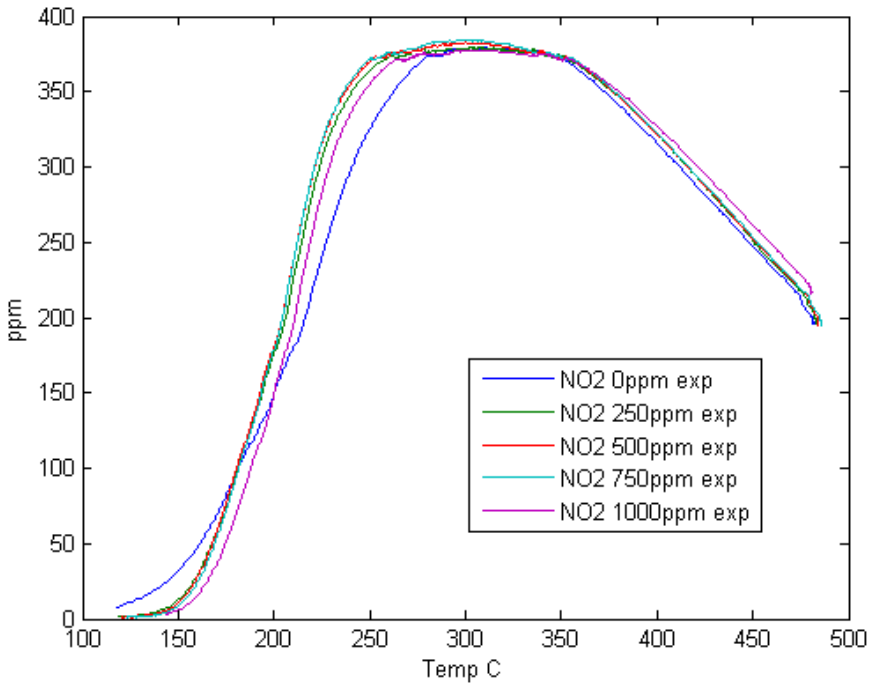

Figure 6: Experimental NO2 yield as a function of catalyst temperature with various H2 concentrations, for NO/O_2 gas mixture experiment.

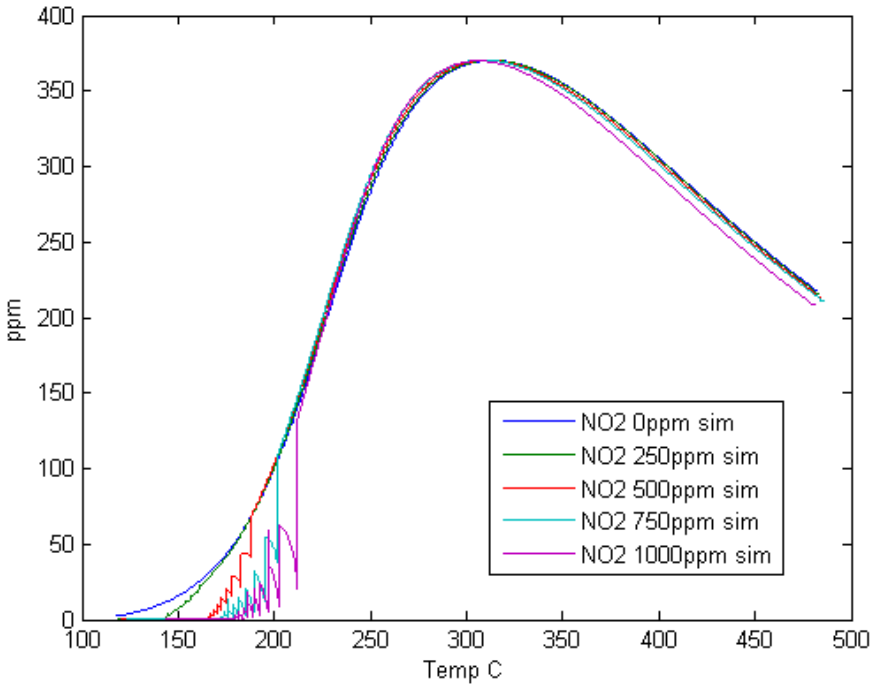

Figure 7: Simulated NO2 yield as a function of catalyst temperature with various H2 concentrations, for NO/O_2 gas mixture experiment.

Figure 7 above shows the simulated NO_2 concentration based on the same experimental conditions as Figure 6. It can be seen that at low temperature, the simulation displays the same delay in NO oxidation light-off with increasing H_2 concentration. Quite a lot of fluctuations can be seen at low temperature, increasingly with increasing H_2 concentration, this can be a result of the large variations in surface coverages at low temperature as well as an effect of N_2O production. At low temperature (130 ˚C with 250ppm H_2 to 180 ˚C with 1000ppm H_2), the model predicts that the platinum surface is mainly covered with dissociated nitrogen N* according to the simulation, which can explain why the light-off occurs at higher temperature compared to the experiment. Indeed, NO oxidation reactions (number 15 and 16) then occur less, since they are dependent on O* coverage, especially the Eley-Rideal mechanism whose activation energy decreases with O* coverage.

From 200˚C to approximately 300˚C NO_2 yield is higher with increasing H_2 concentration, probably due to the retard in platinum oxide formation reported by Azis *et al.* (2015); however the negative effect of H_2 at too high concentration (~1000ppm) only seems to occur between 230 ˚C and 260 ˚C approximately. However all the hydrogen is consumed at less than 200˚C as can be seen in Figure 8, which is consistent with the experiment during which all hydrogen was found to be consumed above 200 ˚C.

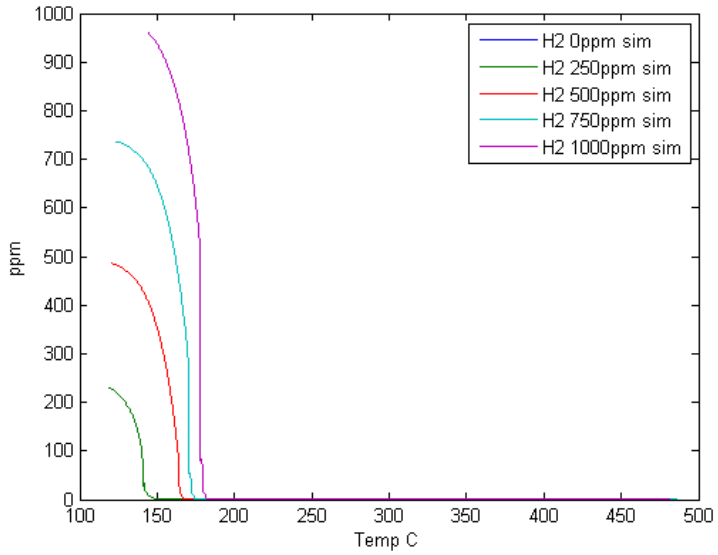

Figure 8: Simulated H2 outlet concentration with various H2 inlet concentrations, for NO/O_2 gas mixture experiment.

Above 300 ˚C, NO_2 yield decreases with the temperature, however it decreases more with increasing H_2 concentrations, as opposed to the experimental results. From 230˚C to 300˚C, NO2 yield is almost the same for each H_2 concentration fed.

4.3.1 N_2O production

Azis *et al.* (2015) experiments also show production of N2O during NO oxidation over Pt/Al2O3. Koop and Deutschmann's (2009) kinetic model predicts production of N2O by reaction of adsorbed N* with NO* (reaction 21 in Table 3). The N* comes from spontaneous dissociation of NO* on platinum or by surface reaction of NO* with H* (reactions 23 and 26 respectively, in Table 3). As will be shown later in Figure 13, without hydrogen in feed, the nitrogen coverage is negligible, therefore very little N* comes from dissociation of NO* (reaction 21).

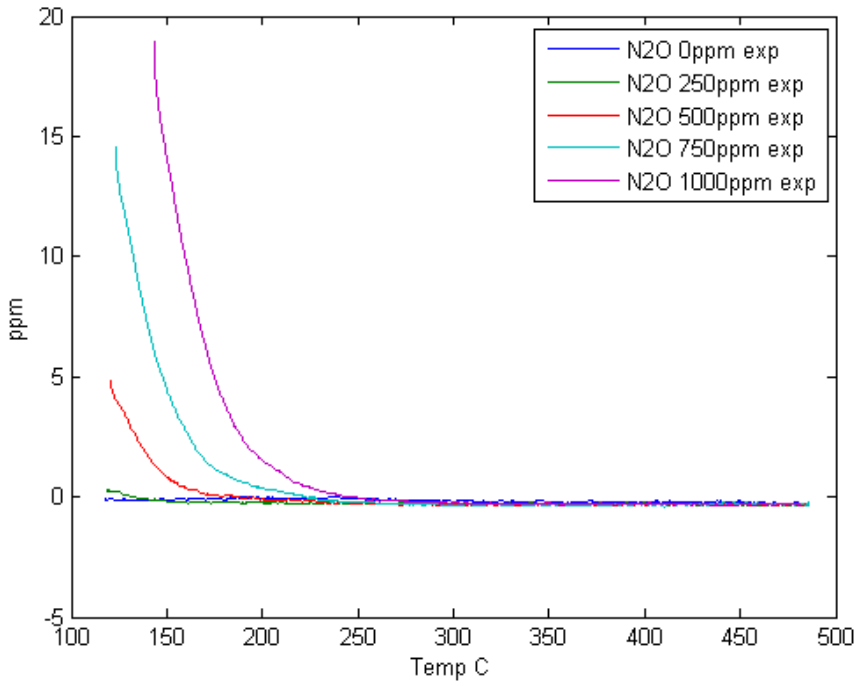

Figure 9: Experimental N2O yield for various H2 concentrations

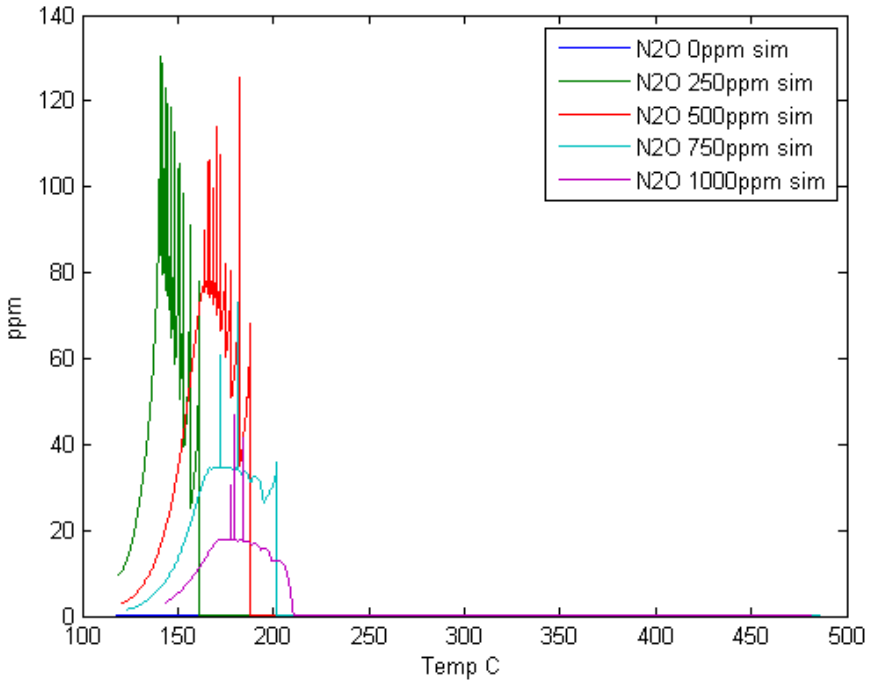

Figure 10: Simulated N2O yield for various H2 concentrations

N_2O formation was observed during experiments only when H_2 was fed in. The corresponding simulated results in Figure 10 show that without H2, there is no formation of N_2O, however experiments show that N_2O yield increase with H_2 concentration and the opposite effect is predicted by the simulation. The reason might be that N_2O is formed by reaction between NO* and N* (reaction 21 in Table 3), but N_2 is formed from reaction of adsorbed nitrogen (reaction 14). As can be seen from comparing Figure 10 and Figure 11, with increasing H_2 concentrations, the model predicts a shift in selectivity from N_2O to N_2.

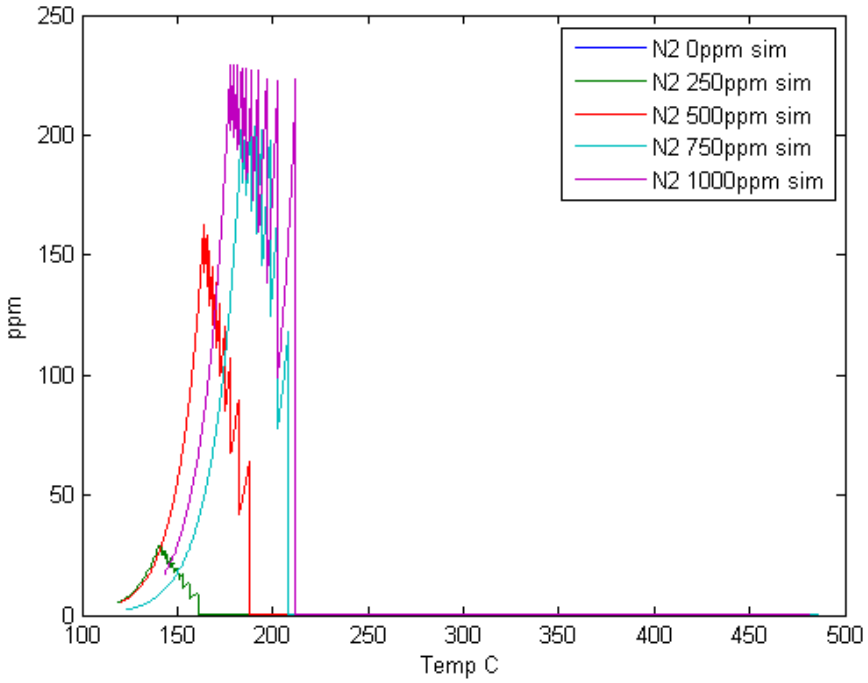

Figure 11: Simulated N_2 concentration for NO/O_2 gas mixture experiment, with various H_2 concentrations in feed.

4.4 Effect of H_2 on Platinum oxide formation

As described in the model building part, Platinum oxide formation is based on the oxidizing effect of NO_2 (reaction 33 in Table 3) and is dissociated by reductive effect of NO (reaction 34 in Table 4). Figure 12 shows the platinum oxide and hydrogen surface coverages for the heating and cooling ramp for both 0ppm and 1000ppm H_2 fed. It can be seen that between 100 and approximately 230˚C, platinum oxide coverage is much lower during the heating ramp when H_2 is fed. Besides, the sudden increase in platinum oxide coverage occurs at ~210˚C and H2 coverage simultaneously drops. Platinum oxide surface coverages during the cooling ramp are roughly the same with or without H_2.

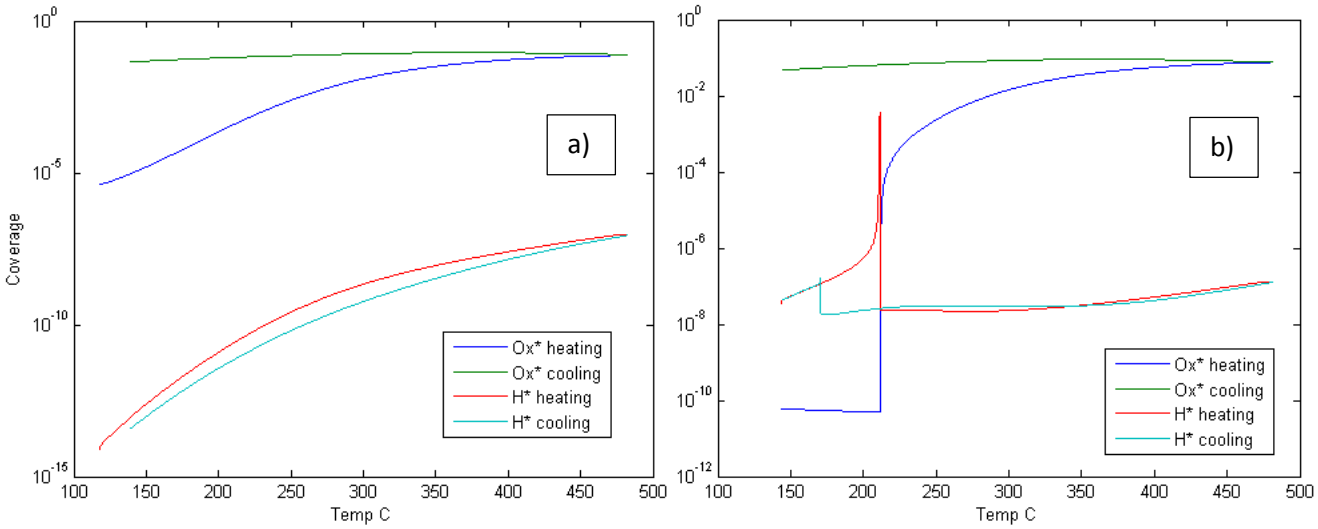

Figure 12: Platinum oxide and hydrogen surface coverage in last tank for NO/O_2 gas mixture experiment, without H2 in feed (a) and with 1000ppm H2 in feed (b)

Our kinetic model does not include any surface reaction between H* and platinum oxide, even though Mulla *et al.* (2006) reported that Platinum oxide is reduced when exposed to H_2. The platinum deactivation delay produced by H_2 in our simulation can mostly be explained by surface coverages. Figure 13 below shows the simulated surface coverages for NO*, O*, NO2*, H*, platinum oxide for 0ppm H2 in feed (a) and 1000ppm (b).

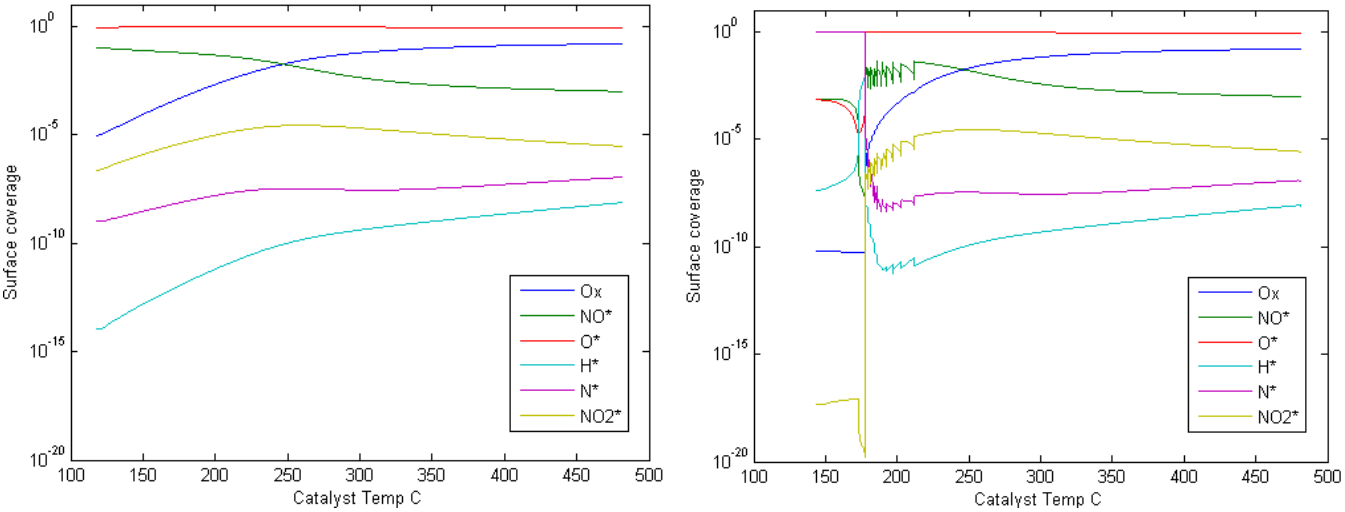

Figure 13: Surface coverages of NO*, O*, NO2*, H* and platinum oxide in last tank. For NO/O_2 gas mixture experiment without H2 in feed (a) and with 1000ppm H2 in feed (b)

At low temperature (below ~220˚C), when H_2 is fed most of the surface is covered by dissociated nitrogen and there is approximately 0.1% of the surface covered with oxygen. This can explain the higher light-off temperature for NO oxidation with H_2 (approximately 30˚C with 1000ppm). Since light-off is delayed, NO_2 yield at low temperature is lower than without H_2 as can be seen in Figure 6 and Figure 7, therefore there is less platinum oxide formed since NO_2 concentration is low. However, no nitrogen was detected during Azis *et al.* (2015) experiments whereas our simulation predicts as much as 230 ppm of N2 produced for the 1000ppm experiment as can be seen in Figure 11. This value seems quite high (approximately 90% conversion of NO into N_2); N_2 production is overestimated by the model

which could partly explain why the light-off temperature from simulation is higher than from experiments when H_2 is fed.

Adsorbed nitrogen is principally produced by reaction 23 and 26 (Table 3), the activation energy of reaction 26 is quite low whereas it is high for reaction 23, and therefore at low temperature reaction 26 will be very fast when H_2 is fed. With high nitrogen coverages, N_2O can be formed by reaction 21.

Above is mentioned the fact that the model in this thesis work does not include hydrogen reactions with platinum oxide, however that would make sense in our model only in temperature ranges where H_2 is not completely converted. At low temperature, our model already predicts that H_2 delays platinum oxide formation, and at higher temperature, H_2 is converted early on inside the reactor. This means reaction with platinum oxide would mostly occur at the entrance of the reactor, hence implementing a reaction between H_2 and platinum oxide might not be necessary.

4.4.1 Transient NO_2 yield at constant T

Figure 14 show the experimental results and simulated NO_2 formation with 0ppm and 750ppm H_2, for the transient experiments as described in the experimental section 2.3. The temporal build-up of platinum oxide is investigated here. Results are scaled within a range of 0 to 1 by dividing by the maximum NO_2 concentration signal over the time range.

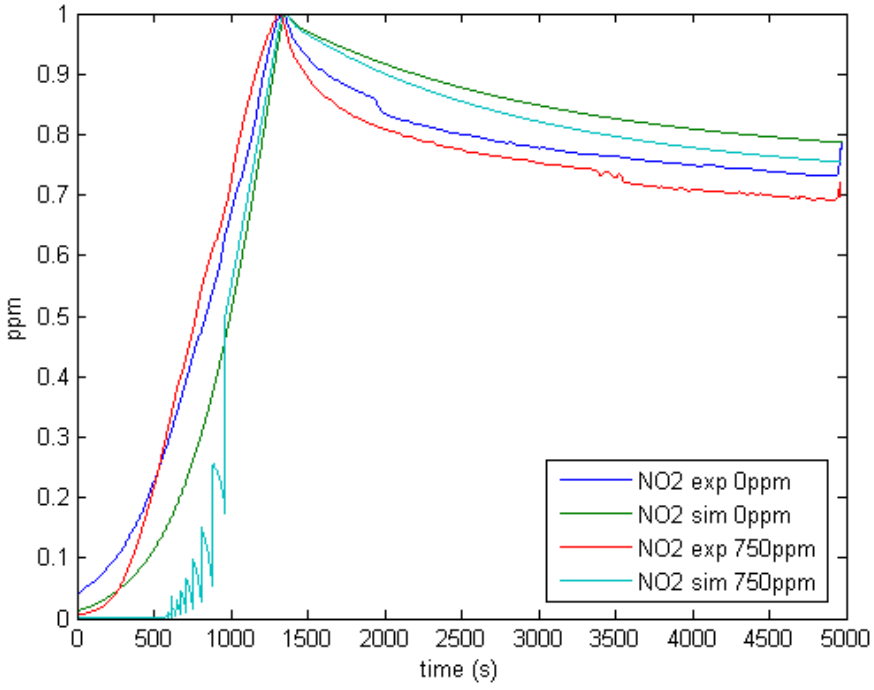

Figure 14: Transient NO2 yield as a function of time, heating up from 120-230˚C with a rate 5˚C/min, then holding 1h at 230˚C, for both simulation and experiment

From the experiments it can be seen that the rate of decay in NO_2 yield increases with H_2, which is observed for the simulation results too. There is approximately a decrease of 21% in NO_2 yield according

to the simulation and -26% according to the experiment. With 750ppm, the decay is -25% for the simulation and -30% for the experiments. The decay increase due to H2 after one hour seems to be roughly the same for both, with a 4% increase in the decay. The fact that the simulated curves are above the experimental ones during the holding up might be due to the fact that platinum oxide build up at 230˚C is underestimated and/or the negative effect of H_2 on platinum oxide formation overestimated.

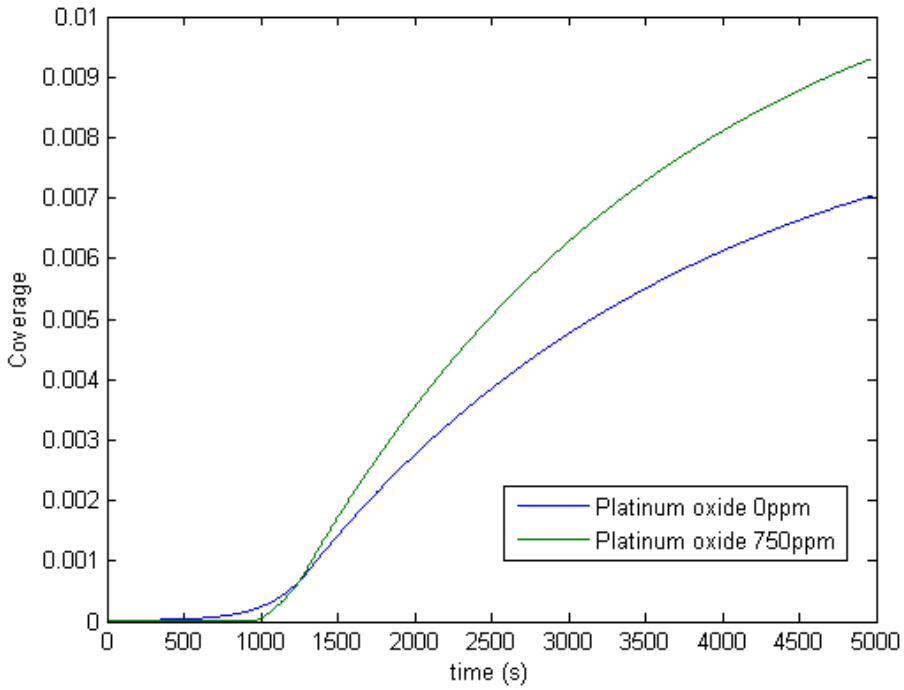

Figure 15: Simulated platinum oxide coverage as a function of time for the same experimental conditions as Figure 14.

Figure 15 above show that the platinum oxide formation is much faster when H2 is fed. When heating up to 230˚C platinum oxide formation is delayed when 750 ppm H2 is fed, but then, once the temperature ramp is stopped, it catches up and then increases faster.

4.5 H_2 effect on the hysteresis behavior

When ramping the temperature up and then ramping down, an inverse-hysteresis effect is observed (Hauptmann *et al.* 2009), meaning that the activity is higher when ramping-up than when ramping down. This name of ‘’inverse’’-hysteresis is due to the fact that most oxidation reactions, such as CO oxidation on platinum, have higher activity when ramping-down than when ramping-up (Salomons *et al.* 2007). This inverse-hysteresis effect is a result of platinum oxide formation, and more precisely to the fact that for transient experiments, the surface platinum oxide coverage lags behind its steady-state value which is the same regardless of ramping up or down (Hauptmann *et al.* 2009). Indeed, platinum oxide formation is relatively slow and it is far from steady-state with the temperature ramp rate used in these experiments.

Azis *et al.* (2015) have investigated the effect of H_2 on this hysteresis behavior and have found that for NO/O_2 mixtures, H_2 increases the hysteresis effect, giving larger hysteresis loops. As can be seen in Figure 16, the experimental hysteresis loop gets bigger with H_2 concentration, but seems to start to get smaller for 1000ppm. The simulated results plotted in Figure 17 show that there is no discernable difference between the hysteresis loops.

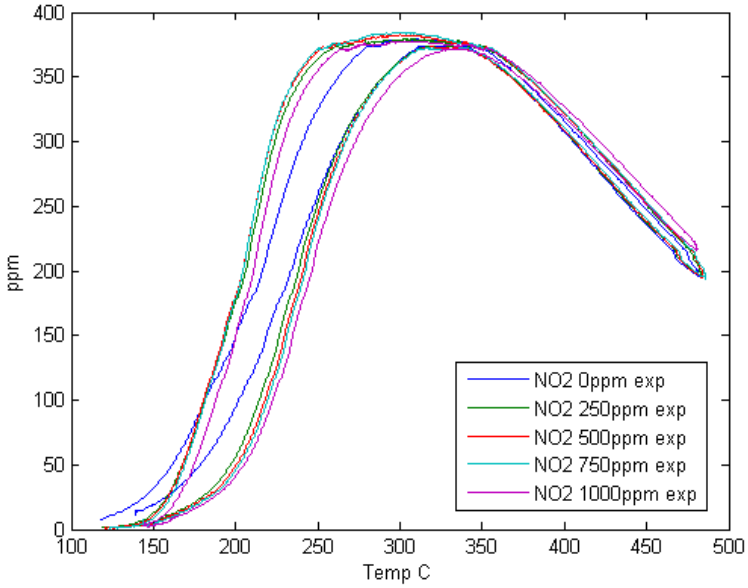

Figure 16: Experimental NO2 hysteresis

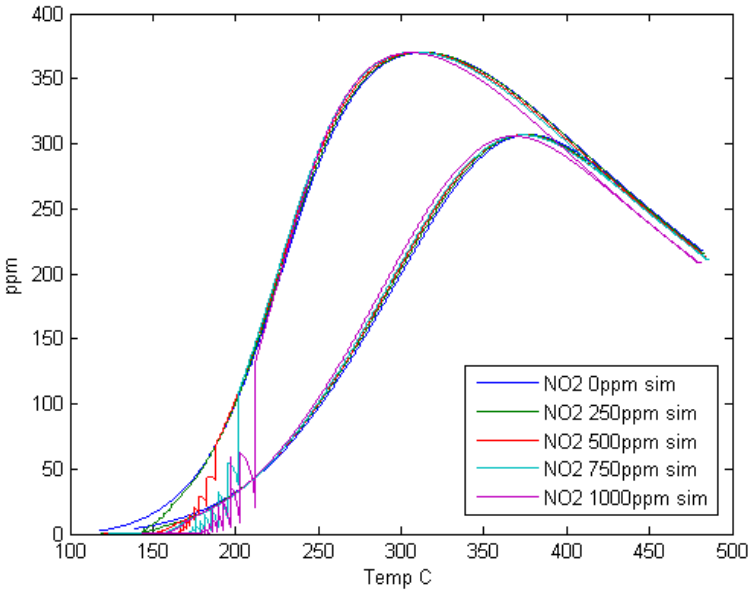

Figure 17: Simulated NO2 hysteresis

As stated previously, the experimental curves show that the hysteresis effect increases with H2 concentration, which can be explained by the fact that at low temperature (200-300˚C), H_2 hinders platinum oxide formation, which combined with surface interaction with NO yield higher NO_2. However, at higher temperature, NO_2 produced oxidize the platinum and since NO_2 yield is higher with H_2 concentration, there is more platinum oxide formed and thus a larger hysteresis.

Simulated results show that the model also predicts a hysteresis behavior; nevertheless H2 seems to have little to no effect on the width of the hysteresis loop. The hysteresis loops predicted by the simulation are however larger than those obtained experimentally. The reason might be that the platinum oxide formation is overestimated by the model, which could be explained by the fact that the model used for platinum oxide formation and dissociation, developed by Hauptmann *et al.* (2009) is based on NO/O2 gas mixtures without any hydrogen fed. Besides, their model is developed for relatively low temperature (80-370˚C), hence maybe not as relevant above this range. The absence of clear differences between the simulated hysteresis loops for different H_2 concentration might be due to the fact that the platinum oxide coverage is roughly the same for temperature higher than 200 ˚C, though slightly higher with higher H_2 concentration as can be seen in Figure 18. H_2 in feed actually causes slight differences for both heating ramp and cooling ramp.

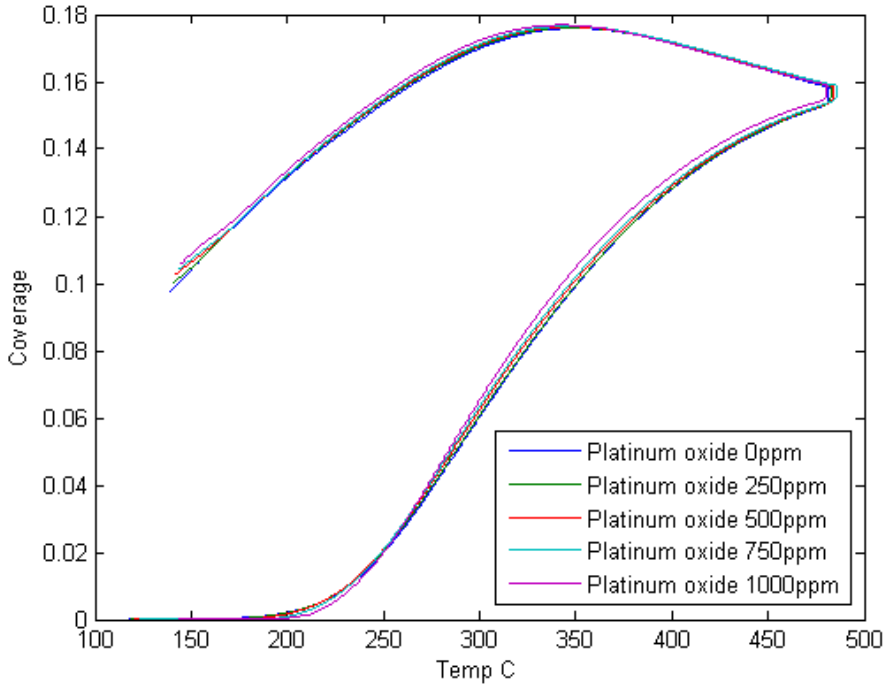

Figure 18: Simulated platinum oxide coverage hysteresis

At low temperature (around 180-220 ˚C) the activity of the cooling ramp is higher than the activity of the heating ramp which is not consistent with the inverse-hysteresis that is observed.

4.6 Effect of H_2 on $NO/O_2/CO$ gas mixtures

Simulations for mixtures with 200 ppm of CO in feed were also performed. The model with CO reactions is much more sensitive, given that 4 adsorbed species, 14 reactions and coverage dependencies are added to the kinetic model. Azis *et al.* (2015) reported that H_2 had little effect on NO_2 yield, at least for light-off temperature, as a marginal increase in the yield between 150-300˚C could still be seen, as shown in Figure 19. CO can be seen to be fully consumed by approximately 135˚C, down to ca. 125˚C for H_2 concentration 750 and 1000ppm.

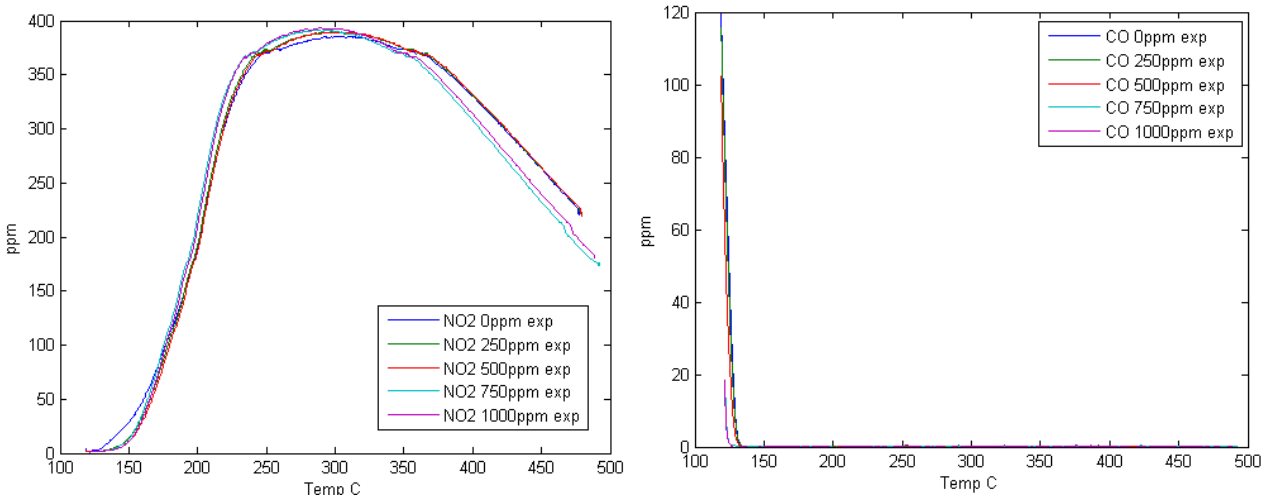

Figure 19: (a) Experimental NO2 yield for NO/O2/CO gas mixtures. (b) Experimental CO outlet concentration.

Simulation results for $NO/O_2/CO$ are shown in Figure 20. NO oxidation light-off temperature seems to be delayed, even without H_2 in feed. Light-off occurs only once CO has been totally consumed. Contrary to experiment, H_2 still has influence over the light-off temperature and the NO_2 yield at low temperature (below 200˚C). Above 200˚C, the behavior is the same as for NO/O_2 mixtures.

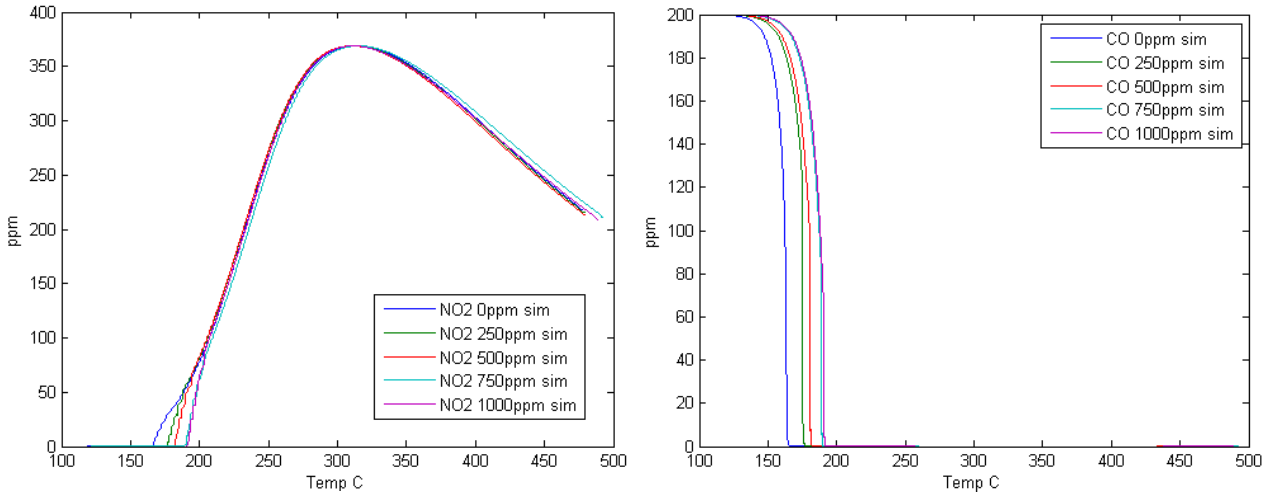

Figure 20: (a) Simulated NO2 yield for NO/O2/CO gas mixtures. (b) Simulated CO outlet concentration.

NO oxidation only occurs once the CO has been entirely consumed because at low temperature, CO occupies most of the platinum sites, as shown in Figure 21. Until ca. 180-200˚C, the surface is covered by CO, then oxygen covers most of it. Contrary to NO/O_2 mixtures, adsorbed nitrogen coverage remains quite low at all temperatures. Platinum oxide profile remains the same as for NO/O_2 mixtures with hydrogen fed, mostly because adsorbed CO acts the same way adsorbed nitrogen acted with NO/O_2 mixtures: denying oxygen adsorption, thus inhibiting NO oxidation until oxygen finally covers most of the sites.

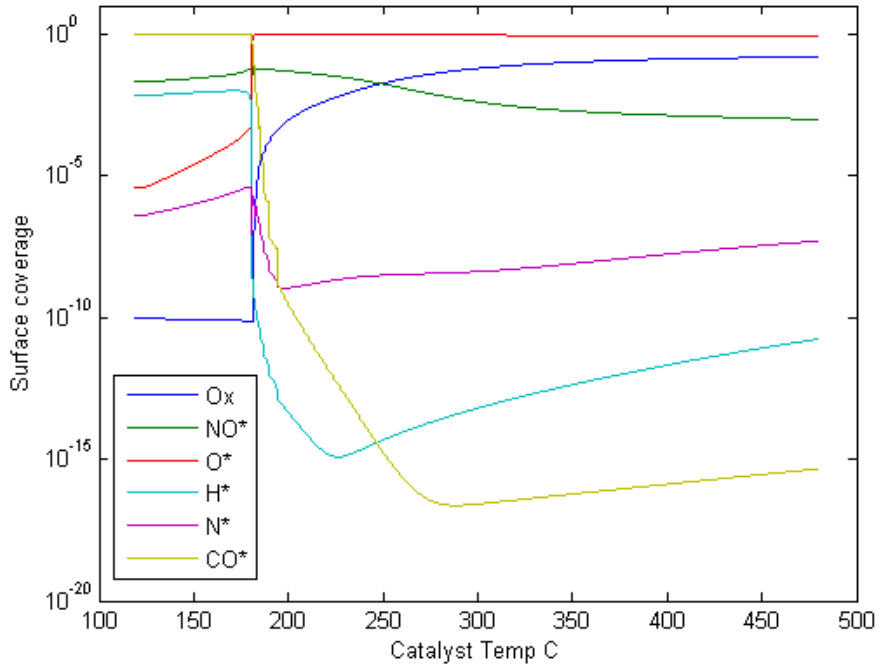

Figure 21: Surface coverage for platinum oxide, NO*, O*, H*, N* and CO* for NO/O_2/CO mixtures with 500 ppm H_2

Compared to the experiments, the light-off temperature for CO oxidation is overestimated by the model, even more with increasing H_2 concentrations whereas this light-off temperature seems to decrease experimentally with CO oxidation. Even without hydrogen fed, the light-off temperature predicted is 30-40˚C higher than observed, as seen in Figure 19 (b) and Figure 20 (b). This inhibition of NO oxidation reaction at low temperature by CO has been reported by Hauff *et al.* (2012), but at much higher concentration: 2500 ppm CO.

Comparing Figure 21 and Figure 22 show that at low temperature, when H_2 is fed, H* and N* coverages are higher than without H_2, and O* coverage increase is slower than without H_2. This lower oxygen coverage might explain why the light-off temperature for CO oxidation is predicted to be so high with the model. Besides, it has been noted that in the case of NO/O_2 gas mixtures, N* coverage was overestimated, hence O* coverage at low temperature with H_2 in the feed might be underestimated. However, it cannot be the only reason, because even without H_2 the light-off temperature predicted by the model for CO is too high.

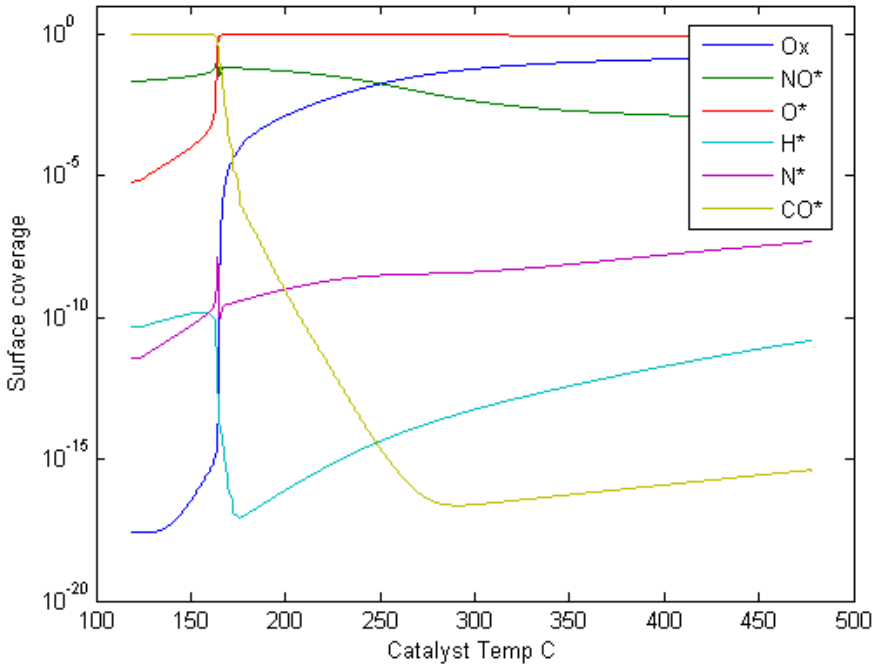

Figure 22: Surface coverage for platinum oxide, NO*, O*, H*, N* and CO* for NO/O2/CO mixtures without H2

5. Conclusion

The purpose of this thesis work was to develop a program to test an existing micro-kinetic model for Diesel oxidation catalyst reactions, and try to see how well it fit the experiments performed by Azis et al. (2015), in order to investigate further the effects of H_2 on DOC. The model was taken from Koop and Deutschmann (2009) and Hauptmann et al. (2009) for platinum oxidation. The model was based on a simple tanks-in-series simulation of a single channel of the monolith, with only axial discretization of the monolith.

From Azis et al. work (2015), this study focused mainly on the NO/O_2 mixtures, and then tried to simulate $NO/O_2/CO$ mixtures, because trying to simulate directly $NO/O_2/CO/C_3H_6$ gas mixtures would have been too complicated and difficult to troubleshoot. For NO/O_2 mixtures, the micro-kinetic model was found to simulate relatively correctly the low temperature light-off delay with increasing hydrogen. Between 200-300˚C, H_2 has no more effect on NO_2 yield, and above 260˚C the decrease in NO2 yield seen experimentally for H_2 concentration of 1000ppm was not reproduced by the model. In the thermodynamic regime (above 300˚C) NO_2 simulated yield is lower with increasing H_2 concentrations as opposed to the experiments. This could be a result of an overestimated platinum oxide formation, which also could explain the too large hysteresis loops obtained. These hysteresis loops remain roughly constant, failing to simulate the increase in the width of the loop with increasing H_2 concentration. N_2O formation was also predicted by the model, though the amount produced is much higher than experimentally measured, which can be explained by the almost total nitrogen coverage resulting from H_2 at low temperature. This nitrogen coverage due to H_2 concentration delays platinum oxide formation, which in turn explains the higher light-off temperature for NO_2 yield. However, this delay being too high might indicate that the effect of H_2 on platinum oxide is overestimated in our model.

The promotional effect of H_2 on $NO/O_2/CO$ mixtures was also investigated, though not as thoroughly as for NO/O_2 gas mixtures. It was found that the model predict much higher light-off temperature for both CO and NO oxidation than observed experimentally. Besides, it fails to simulate the promotional effect of H_2 on CO oxidation, actually predicting the opposite: a negative effect of H_2 on CO light-off temperature. Platinum oxide formation during the TPR was found to be unchanged by the addition of 200 ppm of CO.

6. Recommendations for future work

It is important to mention again the fact that a model from literature (Koop and Deutschmann 2009, Hauptmann et al. 2009) was tested, but no parameter fitting was performed, which would have to be done to fit the experiment better. Indeed, taking a model developed to fit other experimental conditions conducted by different people with different equipment is bound to show at some point deviations from the set of experiment used in this thesis work. Besides, the model was kept as simple as possible; therefore its ability to represent reality is questionable. Future work on this model should include propene reactions to see how well they simulate $NO/O_2/CO/C_3H_6$ gas mixtures. Adding platinum oxide reactions with H_2 and O_2 might also be interesting, though the model already seems to overestimate both platinum oxide formation and the retarding effect of hydrogen. Finally, a more realistic model can be achieved by including mass transport, radial catalyst discretization and a more complex heat balance.

Acknowledgements

My gratitude goes to Derek Creaser, my supervisor, for his valuable help throughout every step of this thesis work. His advises in the choice of the model, the coding and the analysis of the results was of great importance and I am thankful for his constant support and availability. I would also like to thank Muhammad Mufti Azis for letting me use his experimental data and helping implement it in the program, and for allowing me to use his picture as the front page of this thesis work. Special thanks to all my colleagues in the Master student's room for all the good time spent there, these relaxing moments allowed me to be more focused on my thesis. Finally, I want to give a general thank to all the people I have met during my stay in Sweden, who turned this Erasmus year into the best experience of my life.

References

Auvray, X. (2013). Fundamental studies of catalytic systems for diesel emission control, Chalmers University of Technology.

AZIS, M. M. (2015). "Experimental and kinetic studies of H2 effect on lean exhaust aftertreatment processes: HC-SCR and DOC."

Després, J., § (2004). "Catalytic oxidation of nitrogen monoxide over Pt/SiO2." Applied Catalysis B: Environmental **50**(2): 73-82.

Fogler, H. S. (2006). Elements of Chemical Reaction Engineering, Prentice Hall PTR.

Fuglestvedt, J., et al. (2008). "Climate forcing from the transport sectors." Proceedings of the National Academy of Sciences **105**(2): 454-458.

Granger, P. and V. I. Parvulescu (2011). "Catalytic NO x abatement systems for mobile sources: from three-way to lean burn after-treatment technologies." Chemical reviews **111**(5): 3155-3207.

Hauff, K., et al. (2012). "Platinum oxide formation and reduction during NO oxidation on a diesel oxidation catalyst–Experimental results." Applied Catalysis B: Environmental **123**: 107-116.

Hauptmann, W., et al. (2007). "Global kinetic models for the oxidation of NO on platinum under lean conditions." Topics in Catalysis **42-43**(1-4): 157-160.

Hauptmann, W., et al. (2009). "Inverse hysteresis during the NO oxidation on Pt under lean conditions." Applied Catalysis B: Environmental **93**(1–2): 22-29.

Herreros, J. M., et al. (2014). "Enhancing the low temperature oxidation performance over a Pt and a Pt–Pd diesel oxidation catalyst." Applied Catalysis B: Environmental **147**(0): 835-841.

Koop, J. and O. Deutschmann (2009). "Detailed surface reaction mechanism for Pt-catalyzed abatement of automotive exhaust gases." Applied Catalysis B: Environmental **91**(1–2): 47-58.

Kumar, A., et al. (2011). "Microkinetic modeling of the NO-H2 system on Pt/Al2O3 catalyst using temporal analysis of products." Journal of Catalysis **279**(1): 12-26.

Li, X., et al. (2003). "A Study on the Properties and Mechanisms for NO x Storage Over Pt/BaAl2O4-Al2O3 Catalyst." Topics in Catalysis **22**(1-2): 111-115.

Mahzoul, H., et al. (1999). "Experimental and mechanistic study of NOx adsorption over NOx trap catalysts." Applied Catalysis B: Environmental **20**(1): 47-55.

Mulla, S. S., et al. (2005). "NO2 inhibits the catalytic reaction of NO and O2 over Pt." Catalysis Letters **100**(3-4): 267-270.

Mulla, S. S., et al. (2006). "Reaction of NO and O2 to NO2 on Pt: Kinetics and catalyst deactivation." Journal of Catalysis **241**(2): 389-399.

Olsson, L., et al. (2001). "A Kinetic Study of NO Oxidation and NOx Storage on Pt/Al2O3 and Pt/BaO/Al2O3." The Journal of Physical Chemistry B **105**(29): 6895-6906.

Olsson, L. and E. Fridell (2002). "The Influence of Pt Oxide Formation and Pt Dispersion on the Reactions NO2⇔NO+1/2 O2 over Pt/Al2O3 and Pt/BaO/Al2O3." Journal of Catalysis **210**(2): 340-353.

Olsson, L., et al. (2005). "Global kinetic model for lean NO x traps." Industrial & engineering chemistry research **44**(9): 3021-3032.

Rankovic, N., et al. (2011). "Kinetic Modeling Study of the Oxidation of Carbon Monoxide–Hydrogen Mixtures over Pt/Al2O3 and Rh/Al2O3 Catalysts." The Journal of Physical Chemistry C **115**(41): 20225-20236.

Salomons, S., et al. (2007). "On the use of mechanistic CO oxidation models with a platinum monolith catalyst." Applied Catalysis B: Environmental **70**(1–4): 305-313.

Thybaut, J. W. and G. B. Marin (2002). Kinetics of Catalyzed Reactions—Heterogeneous. Encyclopedia of Catalysis, John Wiley & Sons, Inc.

Wang, H.-F., et al. (2009). "NO Oxidation on Platinum Group Metals Oxides: First Principles Calculations Combined with Microkinetic Analysis." The Journal of Physical Chemistry C **113**(43): 18746-18752.

Appendices

Appendix I. Nomenclature

Table 6: Nomenclature

	Description	Unit
A	Pre-exponential factor	s^{-1}
C_{Pt}	Mole of Platinum per unit of volume of catalyst	mol_{Pt}/m^3_{cat}
Cp	Heat capacity	$J.K^{-1}.mol^{-1}$
C_{site}	Sites density on catalyst	site/mg
Ea	Activation energy	$J.K^{-1}.mol^{-1}$
F	Molar flowrate	mol/s
k	Reaction constant	s^{-1}
m_{cat}	Mass of catalyst	mg
$m_{monolith}$	Mass of monolith	mg
M	Molar mass	kg/mol
N_A	Avogadro Number	mol^{-1}
N_{ads}	Number of adsorbed species	unitless
N_{gas}	Number of gas phase species	unitless
N_R	Number of reactions	unitless
r	Reaction rate	s^{-1}
R	Gas constant	$J.K^{-1}.mol^{-1}$
S_0	Sticking coefficient at 0 coverage	unitless
t	Time	s
T	Temperature	K
U_{tot}	Radiation heat transfer coefficient	W/K^4
θ	Surface coverage	unitless
ν	Stoichiometric coefficient	unitless
Γ	Surface site density	$mol_{Pt}.cm^{-2}_{exposed\ Pt}$

Appendix II. Program functions description

Table 7: Program functions description

Function	Description	Output
Fysdata	Called by simulate. Set the physical properties	Fys (structure array)
catdata	Called by simulate. Set the properties of the catalyst: Dispersion, mass, site density.	Cat (structure array)
expdata	Called by simulate. Create a structured array with the experimental data to be simulated	Exp (structure array)
Kinetics	Called by simulate. Set all the kinetics parameters, stoichiometric coefficients and reaction orders for each reaction.	Kin (structure array)
Simpdef	Called by simulate. Defines the simulation parameter such as: number of tanks, relative size of the tanks, tolerance for ODEsolver, timescale of simulation,etc.	Simp (structure array)
Calcest	Called by simulate. Calls for each experiments the Matlab function ode15s to solve the differential equation for mass balance, coverages and heat balance.	tx matrix that contain the primary results (time and variable values) to be resolved by function res.
ODEcalc_init	Called by ode15s and calcest. Calculate reaction rates and differential equations to find steady-state for initial conditions, prior to solving with real experimental times.	x0 matrix containing initial steady-state variables.
ODEcalc	Called by ode15s and calcest. Calculate reaction rates and differential equations for each experimental datapoint.	
r_calc	Called by ODEcalc_init and ODEcalc. Calculate the activation energy by accounting for coverage dependencies and calculate reaction rates.	r matrix containing reaction rates.
r_equil_limit	Called by ODEcalc_init and ODEcalc.	r matrix containing reaction rates.

	Scale down reaction rates of reaction pairs when both the absolute value of the mean of the two rates and the absolute value of the difference is above 10^3.	
eventfun	Called by ode15s. Check if the balances for adsorbed species satisfy the criteria for steady state, if so calculations are stopped.	
Resolve	Called by simulate. Called by simulate after calcest and uses the primary result to solve and create the final results.	res (structure array)
plotter	Called by simulate. Plot the relevant figures.	

Appendix III. Program layout

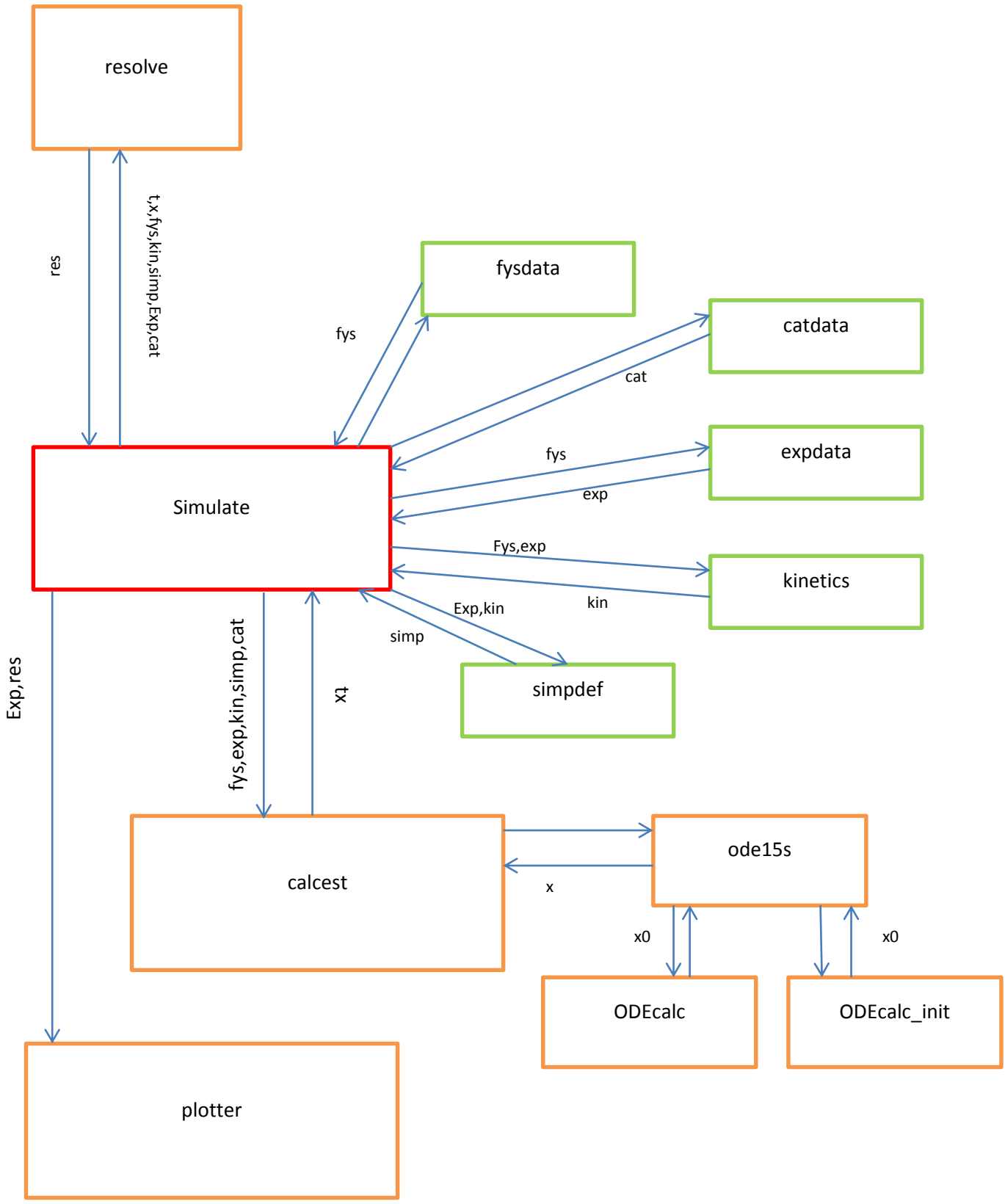

Figure 23: Program layout